Results in Chemistry 7 (2024) 101246

Contents lists available at ScienceDirect

Results in Chemistry

journal homepage: www.sciencedirect.com/journal/results-in-chemistry

Solar photoactive magnesium substituted copper ferrite photocatalysts for Rose Bengal treatment

K.N. Harish [a], Sathish Reddy [b], M.S. Dharmaprakash [a], Sharanappa Chapi [c], B.S. Surendra [d], H.S. Bhojya Naik [e,*], B. Vinay Kumar [f], Anjanapura V. Raghu [g,*]

[a] Department of Chemistry, B.M.S. College of Engineering, Bull Temple Road, Bengaluru, Karnataka 560 019, India
[b] Department of Chemistry, School of Chemical Science, School of Applied Science, REVA Univeristy, Bangalore, India
[c] Department of Physics, B.M.S. College of Engineering, Bull Temple Road, Bengaluru, Karnataka 560 019, India
[d] Department of Chemistry, Dayananda Sagar College of Engineering, Shavige Malleshwara Hills, Kumaraswamy Layout, Bengaluru 560078, India
[e] Department of Studies and Research in Industrial Chemistry, School of Chemical Sciences, Kuvempu University, Shankaraghatta, India
[f] Department of Chemistry, BGS College of Engineering and Technology, Mahalakshmipuram, Bangalore 560086, India
[g] Faculty of Science and Technology, BLDE (Deemed-to-be University), Vijayapura 586103, Karnataka, India

ARTICLE INFO

Keywords:
Solar light
Copper ferrites
Irradiation
PXRD
Energy applications

ABSTRACT

In the present investigation, we have reported solar photo active, cost effective and magnetically recoverable magnesium substituted copper ferrites successfully prepared by simple co-precipitation method. The prepared materials were characterized for structural and microstructural analysis using PXRD, SEM, EDS, FT-IR and UV–Visible spectroscopy. It was observed that, when copper introduces into magnesium ferrite system light absorption shifted to visible region, this is due to formation of metastable energy levels just below the conduction band of magnesium ferrites. As a result an $MgCuFe_2O_4$ catalyst exhibits excellent efficiency under solar light irradiation. These catalysts are stable for longer period even after many runs and magnetically separable. Based on the analysis result these nanomaterials can be used as potential environmental and energy applications under natural sunlight irradiation.

Introduction

In the last several decades, industrial expansion has resulted in an increase in the environmental problem of organic waste and trash accumulation both pollutes the environment and endangers human health. A green method called photocatalysis can be utilized to remove organic contaminants that our highly industrialized civilization has produced [1–4]. Numerous studies have suggested that different organic contaminants can be entirely destroyed through photocatalysis when UV light is used in conjunction with metal oxide semiconductor nanostructures [5–7]. It is common knowledge that solar energy is a renewable resource; yet, because photodegradation processes require UV light, there are currently no industrially applicable sizes where it is viable or advantageous for the environment. This is because the visible light portion of the solar spectrum contains 45 % of the energy, but the UV area only makes up around 4 % of the whole solar spectrum. As a result, creating highly effective visible light photocatalysts for environmental cleanup has been a busy study topic [8–12]. TiO_2 has been extensively studied and is currently a benchmark material for photocatalytic processes. Unfortunately, high-energy ultraviolet (UV) radiation with wavelengths shorter than 388 nm is the only type of UV radiation that can excite TiO_2 semiconductors due to the wide band gap. The development of innovative visible light-responsive photocatalysts with small band gaps, whose absorption wavelength range is expanded into the visible region, is required to increase the efficiency of solar light utilization. Applications for environmental cleanup are actively being researched in such endeavors [13,39,40].

The most significant magnetic materials are ferrites, which also exhibit intriguing photocatalytic capabilities for the evolution of hydrogen or oxygen from water [14–18]. These materials' resistance to photo-corrosion in aqueous solutions and their small band gaps about 2 eV, which permit the absorption of a significant portion of visible light, are desirable qualities for photocatalysts. The main factor in the creation of the narrow band structure is the iron d-orbital. However, they had little activity as single-phase photocatalysts. $MgFe_2O_4$ has garnered a lot of attention and is one of the most significant functional magnetic

* Corresponding authors.
E-mail addresses: hsb25_naik@rediffmail.com (H.S. Bhojya Naik), avraghu23@gmail.com (A.V. Raghu).

https://doi.org/10.1016/j.rechem.2023.101246
Received 4 October 2023; Accepted 1 December 2023
Available online 2 December 2023

materials among the ferrites because of its distinctive qualities of low cost, environmental friendliness, and abundant Mg [19]. The activity of $MgFe_2O_4$ as a single-phase photocatalyst was not very high, despite the material having favorable photo-absorption characteristics. Changing the identity of the divalent M^{2+} cations will alter the characteristics of magnesium ferrite. Metal substitutions can increase the effectiveness of photoinduced charge separation in $MgFe_2O_4$, leading to improved photocatalytic activity.

The creation of a cadmium-substituted $ZnFe_2O_4$ photocatalyst and its outstanding performance in the photocatalytic degradation of MB exposed to natural sun light were covered in the previously reported paper [20]. The reason that photodegradation processes require UV light has limited the usefulness and environmental advantages of solar energy on industrially relevant scales, despite the fact that this renewable energy source is well known. Designing magnetically separable, high-performance visible light photocatalysts has therefore become a very interesting and active research field for environmental cleanup. Given that magnesium ferrite is sensitive to visible light, it is possible to increase the efficiency of degradation under visible light by properly modulating the structure. Copper as a dopant are significant for the photodegradation of organic dyes because they are a carrier of oxygen, the inclusion of Cu and Fe in one compound improves the photocatalytic degradation performance as compared to single Fe_2O_3 and CuO metal oxides [37,38].

The visible-light-induced copper-substituted magnesium ferrites ($Mg_{1-x}Cu_xFe_2O_4$, x = 0.0, 0.25, 0.5 and 0.75) in the current work were made using a straightforward chemical co-precipitation method. $Mg_{0.25}Cu_{0.75}Fe_2O_4$ demonstrated the large photo activity when the photocatalytic activity of $Mg_{1-x}Cu_xFe_2O_4$ was investigated in the degradation of Rose Bengal (RB) under direct sun light exposure. To the best of our knowledge, $Mg_{1-x}Cu_xFe_2O_4$ system is the promising materials for energy and environmental applications.

Experimental section

Materials

Copper nitrate ($Cu(NO_3)_2{\cdot}6H_2O$), magnesium nitrate ($Mg(NO_3)_26H_2O$), ferric nitrate ($Fe(NO)_39H_2O$), and (NaOH) sodium hydroxide were employed as starting materials. The chemical Rose Bengal served as the target for degradation. The analytical grade of each chemical and solvent was used without additional purification.

Catalyst preparation

Cu-substituted chemical co-precipitation method used to create $MgFe_2O_4$ nanostructures with various Cu concentrations [21]. Each starting ingredient was weighed, dissolved in double-distilled deionized water, and then combined in accordance with the formula $Mg_{1-x}Cu_xFe_2O_4$ (where x = 0.0, 0.25, 0.5, and 0.75). As a precipitating agent, drops of sodium hydroxide (GR, 28–30 %) from 3.0 M were gradually added to the salt solution. As the NaOH solution was added drop by drop, the *p*H of the mixture was continuously checked. Until a *p*H of 13 was reached, magnetic stirrer was used to mix the solution continuously. Oleic acid added drop by drop to the solution mixture as the surfactant in the prescribed amount (2–3 drops for a total reacting solution of 75 mL). After stirring the liquid precipitate for 60 min, it was heated to a reaction temperature of 80 °C. The prepared sample was cleaned of undesired contaminants and excess surfactant by cooling the product to room temperature and washing it twice with double-distilled water and ethanol. The stoichiometric amount of the reactants were added from the beginning to control the Cu content (x) in magnesium ferrite.

Characterization techniques

X-ray diffraction techniques with Cu K α-radiation were used to investigate the structure and composition of the $Mg_{1-x}Cu_xFe_2O_4$ ferrite samples. To analyse the morphology of the Mg-Cu ferrite samples, scanning electron microscopy was used with operating at 5.0 kV with model JSM-6700 LV. To identify the chemical compositions Energy dispersive spectroscopy was used. The light response of the prepared ferrites were investigated using UV–visible spectroscopy with a Shimadzu UV-1650 PL model. FTIR was used to determine the impurities/moisture content in the Mg-Cu samples.

Photoactivity studies

The degradation of model organic pollutant Rose Bengal (RB) was used to assess the photoactivity of the synthesized $Mg_{1-x}Cu_xFe_2O_4$ samples. A known volume (50 mL) of Rose Bengal aqueous solution with a concentration of $10mgL^{-1}$ and 0.05 g of $Mg_{1-x}Cu_xFe_2O_4$ nanoparticles were used in each experiment. First the obtained solution was magnetically stirred in the dark for about 30 min to obtain the adsorption/desorption equilibrium. After then, the reaction solution was irradiated to direct sun light outside. To keep the mixture suspended during irradiation, stirring was continued. The reaction mixture was sampled on a regular basis, the $Mg_{1-x}Cu_xFe_2O_4$ nanoparticle catalysts were removed using magnetic separation, and the $Mg_{1-x}Cu_xFe_2O_4$ were then reused for future runs. Using a UV–Vis spectrophotometer to measure absorbance in the 200–800 nm wavelength range, the concentration of each deteriorated solution was tracked over time. As a reference sample, distilled water was employed. After each catalytic run, the $Mg_{1-x}Cu_xFe_2O_4$ was washed and dried to allow for more photoreaction cycles, and the recyclability of $Mg_{1-x}Cu_xFe_2O_4$ was also examined.

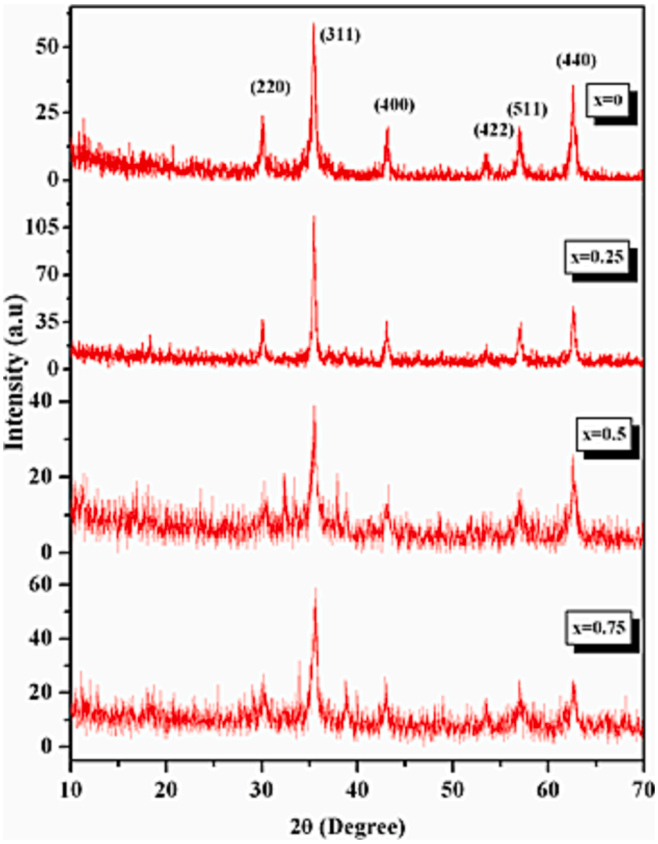

Fig. 1. Comparative XRD patterns of $Mg_{1-x}Cu_xFe_2O_4$ photocatalysts.

Results and discussion

Structural and morphological characterization

Fig. 1 displays the $Mg_{1-x}Cu_xFe_2O_4$ sample powder XRD patterns. Each instance clearly displays the distinctive (440), (511), (422), (400), (311), and (220) reflections of the basic cubic spinel phase. Which shows that the observed products have a Fd3m (SG no.227) cubic spinel ferrite structure, all the diffracted peaks are tallied into a single cubic lattice and the positions and relative intensities of the peaks correspond well with JCPDS card no. 71–1232. All of the samples were examined similarly, and as no impurities found, it may be concluded that none of the prepared samples had any additional structures' diffraction peaks. Scherrer's relation was applied to determine the average crystallite size (D) of Mg-Cu ferrites using the full width at half maximum (FWHM) of the X-ray diffraction peaks. Regarding compositions x = 0.0, 0.25, 0.5, and 0.75, respectively, the typical crystallite diameters were discovered to be 26, 24, 25 and 28 nm.

The lattice parameter was calculated using the formula $(1/d^2_{hkl} = (h_2 + k_2 + l_2)/a^2)$ in accordance with the Fd3m cubic spinel ferrite structure from the strongest (311) reflection. It should be noted that the stepwise introduction of Cu^{2+} ions result in a detectable drop in the lattice parameter a from 0.8406, 0.8390, 0.8380, and 0.8365 nm with regard to x = 0.0, 0.25, 0.5 and 0.75, this can be due to the difference in ionic radius of Cu^{2+} (0.130 nm) and Mg^{2+} (0.142 nm).

Fig. 2 displays the scanning electron microscopic images of the samples with x = 0.0 and x = 0.75 as they were prepared. The outcomes show that a small variation in Cu content causes a small change in the morphology of the samples. The sample's surface morphology at x = 0.75 exhibits a finely organized morphology. Both examples, however, demonstrate that some small particles can agglomerate to generate larger particles.

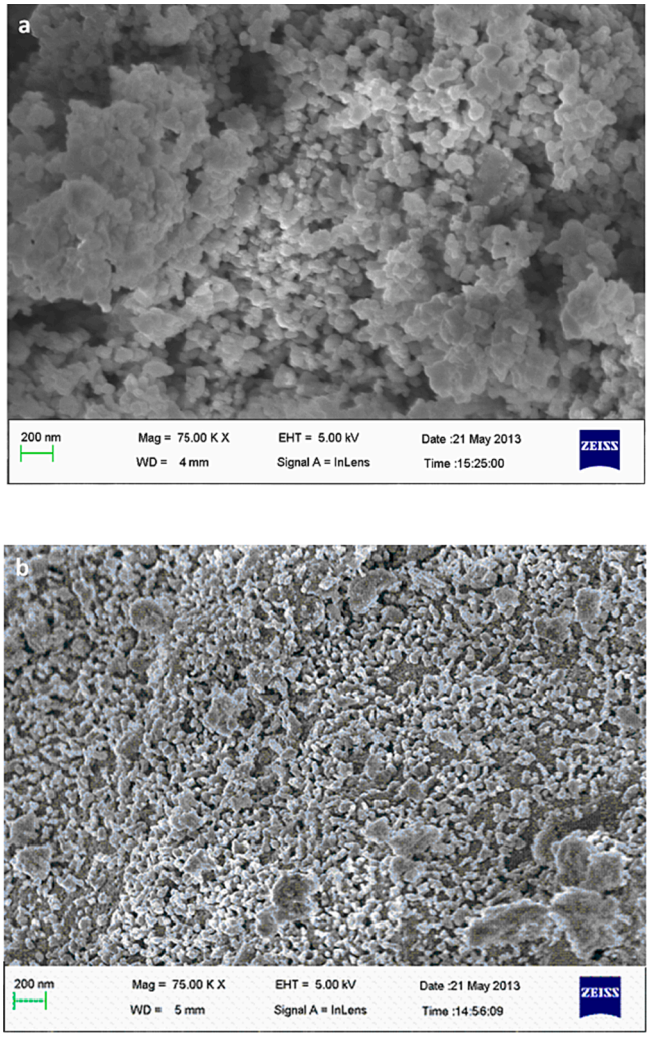

Fig. 2. SEM micrographs of $Mg_{1-x}Cu_xFe_2O_4$ samples, (a = 0.0, b = 0.75).

Fig. 3 **(a)** and **(b)** shows the EDS spectrum of artificial photocatalysts. Mg, Fe, Cu, and O atoms were the samples' main chemical constituents. In the samples with x = 0.0 and 0.75, the majority of the photocatalysts had 15.72 At% Mg and 35.25 At% Fe, respectively, as well as 6.4 At% Mg, 10.45 At% Cu, and 40 At% Fe. The compositional homogeneity and production of the $Mg_{1-x}Cu_xFe_2O_4$ nanocatalysts synthesized by coprecipitation technique were confirmed by the EDS results, which were consistent within experimental stoichiometric ratio with little experimental error. The high photocatalytic effectiveness and large amount of Cu in sample x = 0.75 as compared to x = 0.0 suggest proper preparation. The substantial amount of Fe, meanwhile, enables the photocatalyst to recover better and has strong magnetic properties.

Optical absorption studies

UV–visible absorption studies were conducted to gather crucial data regarding the impact of Cu content on the optical characteristics of Mg-Cu ferrites. The samples' UV–vis spectra are displayed in Fig. 4. The visible light absorption of $Mg_{1-x}Cu_xFe_2O_4$ (x = 0.0, 0.25, 0.5 & 0.75) was boosted and the absorption edge of samples has a considerable red shift, as shown in Fig. 4 with the replacing Cu content.

The sample at x = 0.75 displayed the biggest red shift and the strongest overall light response in the visible region when compared to other samples. The $MgFe_2O_4$ with Cu as a replacement was therefore visible light sensitive. A narrowing of the band gap may explain the increased absorption of visible light. It's possible that the excitation of an electron from the O-2p level into the Fe-3d state is what causes Mg-Cu ferrite to absorb light in the visible spectrum [22].

The band gap between O-2p level and Fe-3d level in magnesium ferrite was found that 2.3 eV, whereas with increase in the copper concentration the energy band gap of O-2p and Fe-3d level decreases as 2.05, 1.98 and 1.8 eV with respect to x = 0.25, 0.5 and 0.75 as depicted in the Fig. 5. Copper substitution could form a dopant energy level within the energy gap of $MgFe_2O_4$. The electronic transitions from the VB to the dopant level or from the dopant level to the CB could effectively lower the electron-hole pair recombination rate, which shifts the broad absorption band toward the visible light region [20]. As a result of formation of metastable energy levels make Mg-Cu ferrites utilize more percent of sunlight. Therefore, Mg-Cu ferrites a better photocatalytic capability under natural sunlight was expected.

Band gap studies

Using the general relation, the optical band gap (E_g) of $Mg_{1-x}Cu_xFe_2O_4$ catalysts was calculated from the absorbance spectra, where a sharp increase in the absorption was seen attributed to the band-band transition. By applying the fundamental connections to the absorption data, the $Mg_{1-x}Cu_xFe_2O_4$ nanoparticle catalysts' absorption coefficient has been calculated [23–25].

$$I = I_0 e^{\alpha t} (1)$$

$$A = \log(I_0/I) (2)$$

and

$$\alpha = 2.303(A/t) (3)$$

where, t is the sample's thickness and A is the absorption for the $Mg_{1-x}Cu_xFe_2O_4$ samples. Tauc plots were used to display $(\alpha h\nu)^{1/n}$ *verses* photon energy ($h\nu$) for several values of n (n = 1/2, 3/2, 2, and 3) in

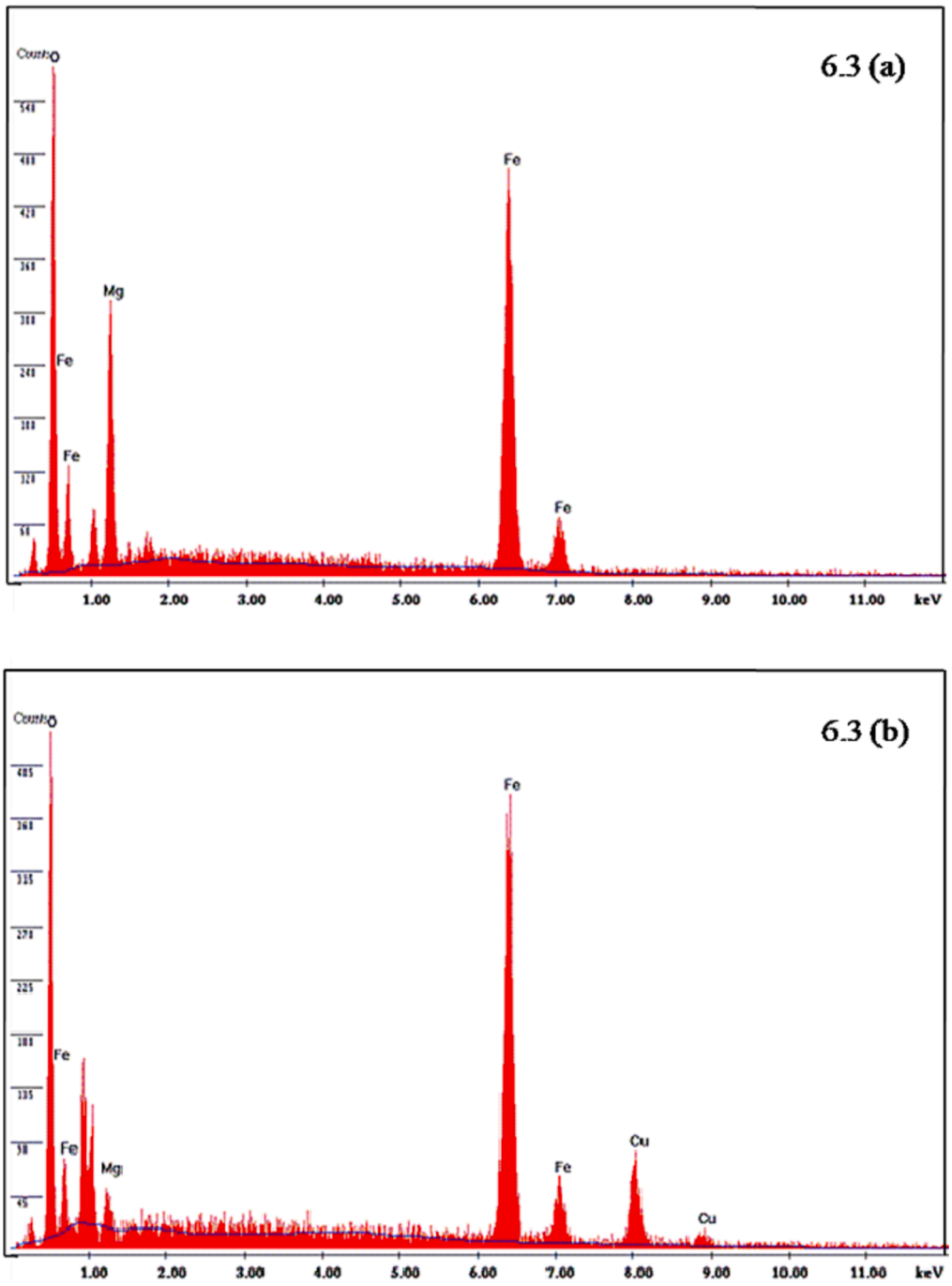

Fig. 3. Energy-dispersive spectra's of x = 0.0 (a) and x = 0.75 (b) samples.

order to find out the band gap of synthesized photocatalysts [26]. The $Mg_{1-x}Cu_xFe_2O_4$ ferrite nanoparticles had the best linear fit when n = 1/2, indicating a direct permitted optical transition. Fig. 5 displayed the Tauc plot. Using software for linear regression, a straight line fit with a very small standard deviation was obtained for the $(\alpha h\nu)^{1/n}$ vs. $h\nu$ plot. The optical absorption edge's value can be found from the line's intercept at $\alpha = 0$. Fig. 5 illustrates how the optical band gap changes as composition x changes. It was found that the band gap narrows as the copper concentration rises. With Cu^{2+} ion concentration increase, the estimated energy gaps of Mg-Cu ferrites steadily decrease from roughly 2.3 to 2.05, 1.98, and 1.8 eV.

The band gap of magnesium ferrite was estimated 2.3 eV. This band gap value was similar to the value reported in the literature [27]. With the substitution of Cu, the energy gap of $MgFe_2O_4$ was redshifted. Additionally, it is clear that when the amount of copper substitution increases, the redshift also increases. Changes in the electrical structure of $MgFe_2O_4$ and the quantum size effect are the two main factors that may affect band gap energies.

In our co-precipitation nanoparticulated samples, since the size of the agglomerated particles was larger than the exciton Bohr radius of bulk ferrite nanoparticles, the sample has a weak quantum confinement as referred in Wu et.al, [28] the interface of nanoparticles obviously contains many oxygen vacancies and may be a source of trapped exciton states that form a series of metastable energy levels within the energy gap, resulting in the red shift of the apparent optical band gap [22,29].

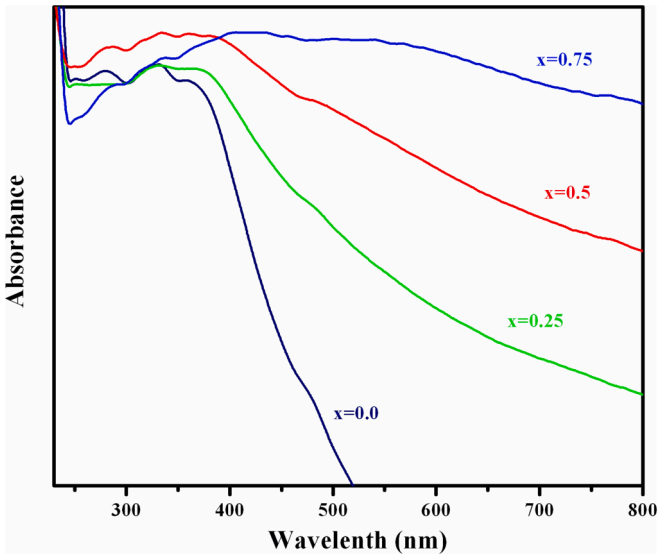

Fig. 4. UV–visible spectra of $Mg_{1-x}Cu_xFe_2O_4$ photocatalysts.

Photocatalytic activity

As per the experimental findings of investigations on UV–visible absorption, the current Mg-Cu ferrite samples possess the essential property for photocatalytic destruction of organic molecules. For the investigation of catalytic performance, Rose Bengal (RB) was typically chosen as the model organic pollutant. First, two different types of studies have been studied to verify the photodegradation capability of Mg-Cu ferrite samples. One is the blank experiment, which showed that, in the absence of catalysts and under solar illumination, very little RB was directly photolyzed.

In addition, $Mg_{1-x}Cu_xFe_2O_4$ was employed as the starting solution (t = 0 min) in the adsorption–desorption equilibrium solution of the RB. The drops in dye concentration due to adsorption and direct photolysis should be subtracted in order to obtain the true photodegradation yield caused by photocatalysis in the presence of catalysts. After the adsorption equilibrium was reached, the drop brought on by adsorption could be subtracted. Therefore, photodegradation yield was defined as [30]:

$$photodegradation\ yield = \frac{C_o - C_a - C_b}{C_o} \times 100$$

where Co is the dye's initial concentration, Ca is its concentration after being photodegraded, and Cb is its concentration after being directly exposed to light.

Fig. 6 displays the rates of Rose Bengal (RB) photodegradation on

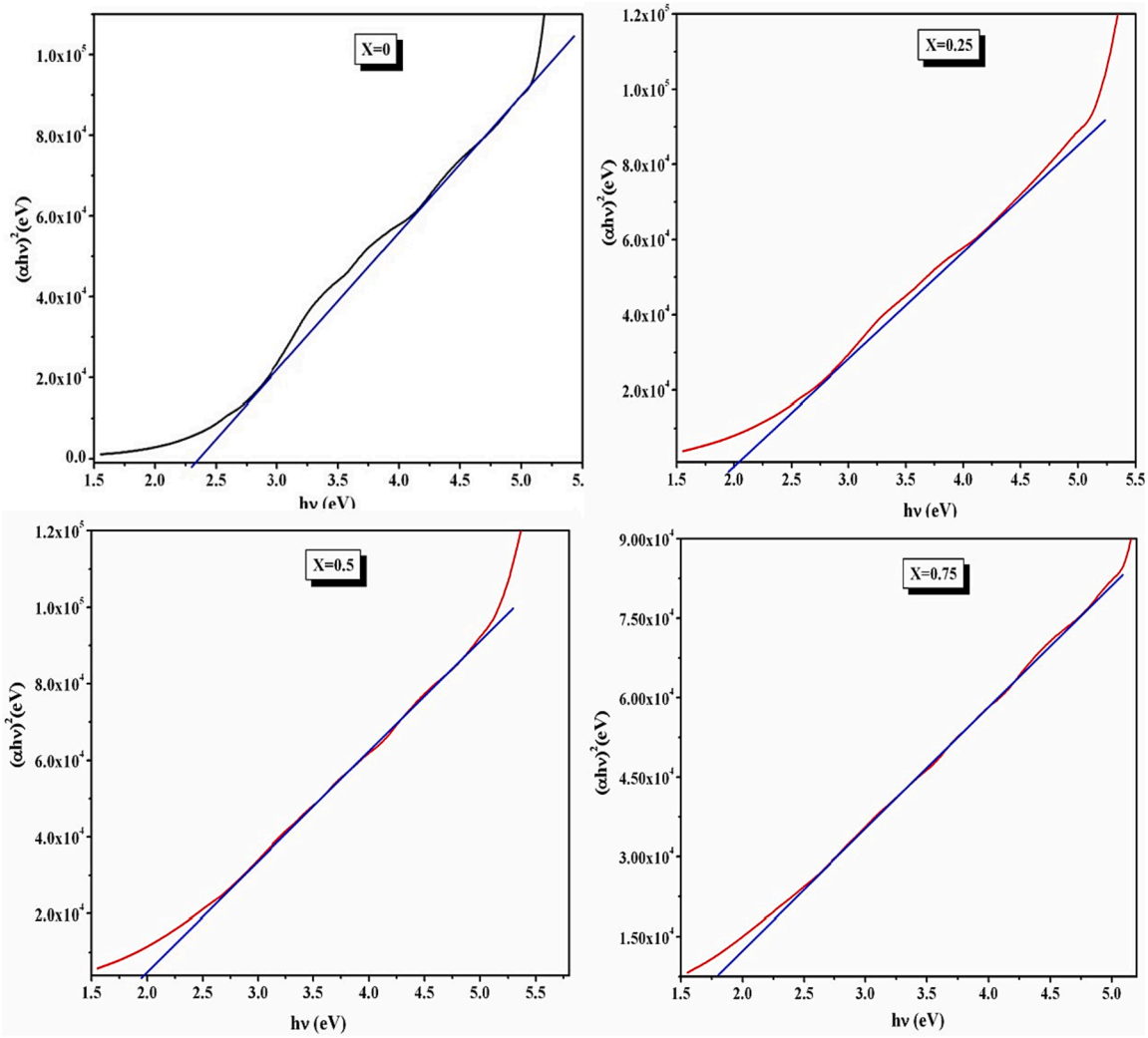

Fig. 5. Plot of $(\alpha h\nu)^2$ as a function of photon energy ($h\nu$) for $Mg_{1-x}Cu_xFe_2O_4$ compositions.

$Mg_{1-x}Cu_xFe_2O_4$ catalysts under exposure to natural sunlight at various time intervals. Fig. 6 illustrates that although Cu-substituted $MgFe_2O_4$ nanoparticles are more effective at eliminating the RB than $MgFe_2O_4$, RB did not appear to decay clearly without a catalyst. With increasing Cu content, the photoactivity of $Mg_{1-x}Cu_xFe_2O_4$ (x = 0.0, 0.25, 0.5, 0.75) were enhanced gradually. The photodegradation activity of the Cu-substituted $MgFe_2O_4$ samples increases with an increase in the Copper substitution level. It was observed that Mg-Cu catalysts with a Cu content of x = 0.75 show the highest photocatalytic activity.

The photocatalytic activity of $Mg_{1-x}Cu_xFe_2O_4$ (x = 0.0, 0.25, 0.5, and 0.75) steadily increased with increasing Cu content. The samples of Cu-substituted $MgFe_2O_4$ exhibit an increase in photocatalytic activity with increasing Cu substitution levels. The maximum photocatalytic activity is demonstrated by Mg-Cu catalysts with Cu contents of x = 0.75, as can be seen.

As seen in Fig. 6, the photocatalyst at x = 0.75 has a better efficiency in comparison with other samples (x = 0.0, 0.25, and 0.5) due to its greater capacity to absorb visible light. In comparison with other ferrite samples (band gaps 2.3 to 1.98 eV), the catalyst at x = 0.75 has a small band gap energy (1.8 eV), because a new energy band appeared just below the conduction band. This new energy band was primarily derived from the electronic states of the introduced copper ion (i.e., energy level of introduced copper), which led to a decrease in the rate of electron-hole recombination. The total number of electrons entering the conduction band increases due to the reduced energy band gap, resulting in a comparatively high electron density in the conduction band. Consequently, in the valence band, the number of holes also increases. In order to create OH• Radicals, these electrons and holes interact with surface-bound H_2O or OH^-. Since OH• free radicals were the primary active species during the photocatalytic degradation process, this encourages the creation of more of them [31–33].

Mechanism of photocatalytic degradation

Based on the results and literature reports [34,35] a possible mechanism of photodegradation over $Mg_{1-x}Cu_xFe_2O_4$ nanoparticles were discussed as depicted in the Scheme 1. In comparison, pure magnesium ferrite hardly excited by visible light due to large energy band gap (2.3 eV), as a result low efficiency in photodegradation. The modification of magnesium ferrite by substituting copper results in high visible light absorption due to the new energy levels are formed within conduction band of $MgFe_2O_4$. These energy levels are just below the conduction band edge. Upon exposed to natural sun light irradiation electrons are excited from valence band to energy levels of $Mg_{1-x}Cu_xFe_2O_4$ system (conduction band) as shown in Scheme 1, simultaneously same amount of holes are generated at the valence band. Meantime, it is highly possible for the generated photo-electrons to jump from high energy level conduction band of $MgFe_2O_4$ to low energy levels of $Mg_{1-x}Cu_xFe_2O_4$ system. As a result, recombination of photogenerated electrons and holes can be minimized.

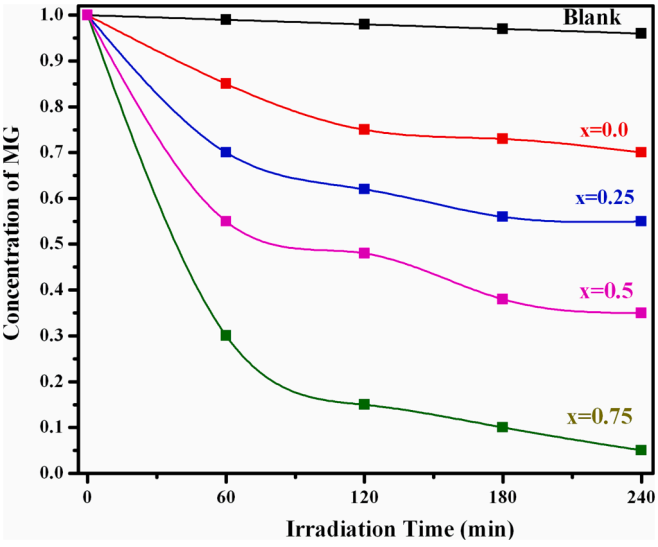

Fig. 6. Degradation of Rose Bengal (10.0 mg L^{-1}) with different $Mg_{1-x}Cu_xFe_2O_4$ system under natural sun light irradiation.

The photo-induced holes produce $OH^•$ radical species by directly reacting with organic dyes or interact with surface bound H_2O or OH^-. These free radicals act as a strong oxidant for the removal of organic pollutants from water. At the same time, the photogenerated electrons react with adsorbed molecular oxygen to produce $O^•{}_2^-$. As generated $O^•{}_2^-$ combines with H^+ to produce $HO_2^•$, further this active species reacts with trapped electrons to produce $OH^•$ radical. The as generated $OH^•$, $HO_2^•$, $O^•{}_2^-$ and holes are highly reactive species which could oxidize the organic pollutants present in the water. On the basis of the above analysis, photo-catalytic reactions expressed as follows [36–38],

$$Mg_{1-x}Cu_xFe_2O_4 + h\nu \rightarrow Mg_{1-x}Cu_xFe_2O_4\ (e^-_{cb} + h^+_{vb}) \rightarrow Mg_{1-x}Cu_xFe_2O_4 + \text{Energy} \quad (4)$$

$$Mg_{1-x}Cu_xFe_2O_4\ (h^+_{vb}) + H_2O \rightarrow H^+ + OH^• \quad (5)$$

$$Mg_{1-x}Cu_xFe_2O_4\ (h^+_{vb}) + OH^- \rightarrow OH^• \quad (6)$$

$$Mg_{1-x}Cu_xFe_2O_4\ (e^-_{cb}) + O_2 \rightarrow O^•{}_2^- \quad (7)$$

$$O^•{}_2^- + H^+ \rightarrow HO_2^• \quad (8)$$

$$2e^-_{cb} + HO_2^• + H^+ \rightarrow OH^• + OH^- \quad (9)$$

$$OH^•, HO_2^•, O^•{}_2^-, h^+_{vb} + \text{Organic pollutants} \rightarrow \text{Degradation product} \quad (10)$$

Recyclability

By reactivating the utilized catalysts four times, the reusability of the catalyst was investigated. The $Mg_{1-x}Cu_xFe_2O_4$ photocatalysts perform well in magnetic separation using $MgFe_2O_4$ due to its good magnetic characteristics (see the inset of Fig. 7 for more information), and the catalyst can be reused four times. It has been noted that even after recycling four times, the rate of the RB's photocatalytic reaction over the $Mg_{0.25}\ Cu_{0.75}\ Fe_2O_4$ sample nearly stays the same. These findings support the notion that the Mg-Cu ferrites created during the current investigation were very efficient visible-light-induced photocatalysts for the RB molecules' degradation.

Conclusion

The study offered a useful method for making copper-substituted magnesium ferrite photocatalysts driven by solar light. The band gap of $Mg_{1-x}Cu_xFe_2O_4$ (x = 0.0, 0.25, 0.5, 0.75) ferrites steadily reduce with an increase in Cu content, and the lower band gap of ferrites results in an improved photocatalytic activity for RB degradation when exposed to solar light. Particularly, when compared to pure $MgFe_2O_4$, the $Mg_{0.25}Cu_{0.75}Fe_2O_4$ sample demonstrates much better photocatalytic activity. This study's strategy for creating multicomponent magnetic ferrite materials with desirable visible-light photocatalytic activity was shown to be very beneficial. In terms of their inherent qualities, such as high chemical stability and great resistance to acid and alkali, it is believed that such a novel class of the photocatalysts were promising materials for practical application in the field of visible light induced photodegradation of organic pollutants.

Funding

This research did not receive any specific grant from funding

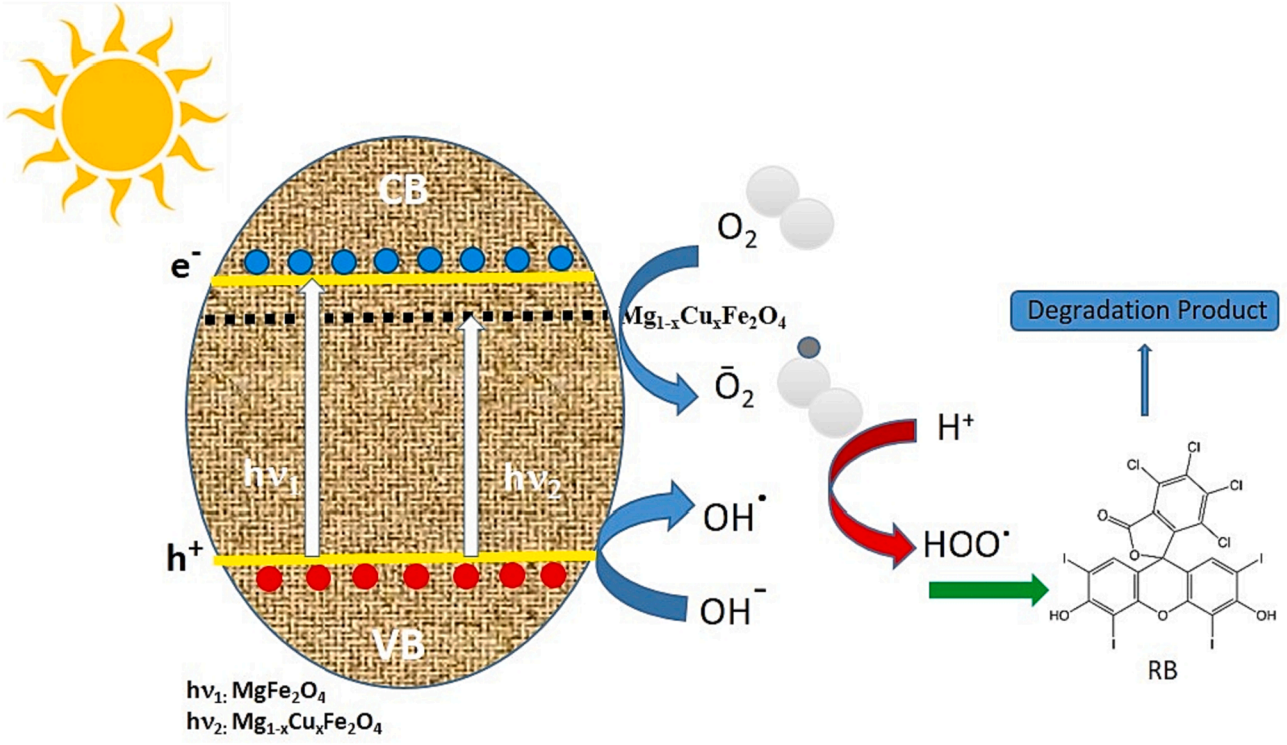

Scheme 1. Photocatalytic mechanism of $Mg_{1-x}Cu_xFe_2O_4$ system under natural sun light irradiation.

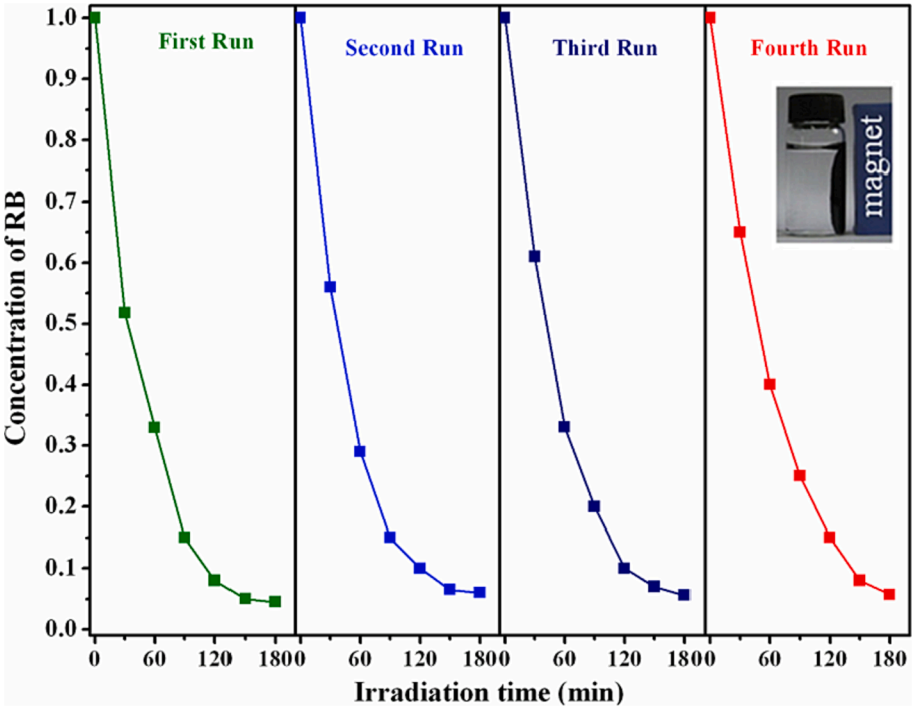

Fig. 7. The photodegradation rate of RB in solution for 4 cycles using Mg_{1-x} $Cu_xFe_2O_4$ (sample at x = 0.75) phatalyst under natural light irradiation and the inset figure reveals the magnetic separation property of $Mg_{1-x}Cu_xFe_2O_4$ nanoparticle catalysts.

agencies in the public, commercial, or not-for-profit sectors.

Data availability Data will be made available on request.

CRediT authorship contribution statement

K.N. Harish: Writing – original draft. **Sathish Reddy:** Visualization. **M.S. Dharmaprakash:** Funding acquisition. **Sharanappa Chapi:** Conceptualization. **B.S. Surendra:** Resources. **H.S. Bhojya Naik:** . **B. Vinay Kumar:** Supervision. **Anjanapura V. Raghu:** Project administration, Supervision.

Declaration of competing interest

The authors declare that they have no known competing financial interests or personal relationships that could have appeared to influence the work reported in this paper.

Data availability

Data will be made available on request.

Appendix A. Supplementary data

Supplementary data to this article can be found online at https://doi.org/10.1016/j.rechem.2023.101246.

References

[1] S. Kumari, N. Dhanda, A. Thakur, V. Gupta, S. Singh, R. Kumar, S. Hameed, P. Thakur, Ceram. Int. 49 (8) (2023) 12469–12480.
[2] P. Ramadevi, R.a. Shanmugavadivu, R. Venkatesan, J. Mayandi, S. Sagadevan, Inorg. Chem. Commun. 150 (2023), 110532.
[3] V.D. Sonu, A. Sudhaik, A.A.P. Khan, T. Ahamad, P. Raizada, S. Thakur, A.M. Asiri, P. Singh, Mater. Res. Bull. 164 (2023), 112238.
[4] C. Maria Magdalane, G. Maria Assuntha Priyadharsini, K. Kaviyarasu, A. Irudaya Jothi, G. Gnanamani Simiyon, Surfaces and Interfaces, 25, **2021**, 101296.
[5] Deepika Chahar, Shilpa Taneja, Shalini Bisht, Shubhi Kesarwani, Preeti Thakur, Atul Thakur, P.B. Sharma, Journal of Alloys and Compounds, 851, **2021**, 156878.
[6] S.A. Jadhav, M.V. Khedkar, S.B. Somvanshi, K.M. Jadhav, Ceram. Int. 47 (20) (2021) 28623–28633.
[7] A. Nawaz, A. Khan, N. Ali, N. Ali, M. Bilal, Environ. Technol. Innov. 20 (2020), 101079.
[8] Z.J. Zhang, W.Z. Wang, W.Z. Yin, M. Shang, L. Wang, S.M. Sun, Appl. Catal. B 101 (2010) 68.
[9] Y.Y. Liang, H.L. Wang, H.S. Casalongue, Z. Chen, H.J. Dai, Nano Res. 3 (2010) 701.
[10] B.K. Vijayan, N.M. Dimitrijevic, J.S. Wu, K.A. Gray, J. Phys. Chem. C 114 (2010) 21262.
[11] N. Romcevic, R. Kostic, B. Hazic, M. Romcevic, I. Kuryliszyn- Kudelska, W. D. Dobrowolski, U. Narkiewicz, D. Sibera, J. Alloy. Compd. 507 (2010) 386.
[12] Y. Fu, P. Xiong, H. Chen, X. Sun, X. Wang, Ind. Eng. Chem. Res. 51 (2012) 725.
[13] H. Zhang, G. Chen, D.W. Bahnemann, J. Mater. Chem. 19 (2009) 5089.
[14] Hebah Sami Jarusheh, Ahmed Yusuf, Fawzi Banat, Mohammad Abu Haija, Giovanni Palmisano, Journal of Environmental Chemical Engineering, 10, 5, **2022**, 108204.
[15] Y. Matsumoto, M. Omae, K. Sugiyama, E. Sato, J. Phys. Chem. 91 (1987) 577.
[16] M. Sun, X. Han, S. Chen, Mater. Sci. Semicond. Process. 91 (2019) 367–376.
[17] S. Swathi, R. Yuvakkumar, P. Senthil Kumar, G. Ravi, D. Velauthapillai, Chemosphere 281 (2021), 130903.
[18] H.M. Sundararajan, B. Bonisha, M. Ubaidullah, M.F. Shoyeb, S. Shaikh, D. Revathi, A.T. Thiripurasundari, B. Pandit, Chandra Sekhar Dash, MohdShahazad, Mater. Res. Bull. 154 (2022), 111911.
[19] R. Koferstein , T. Walther , D. Hesse , S. G. Ebbinghaus, *J. Mater. Sci*, **2013**, DOI 10.1007/s10853-013-7447-x.
[20] K.N. Harish, H.S. Bhojya Naik, P.N. Prashanth kumar, R. Viswanath, Catal. Sci. Technol. 2 (2012) 1033.
[21] K. Maaz, S. Karim, A. Mashiatullah, J. Liu, M.D. Hou, Y.M. Sun, J.L. Duan, H.J. Yao, D. Mob, Y.F. Chen, J. Magn. Magn. Mater. 321 (1838) 2009.
[22] S. Xu, D. Feng, W. Shangguan, J. Phys. Chem. C 113 (2009) 2463.
[23] M. Pathan, J.D. Desai, C.D. Lokhande, Appl. Surf. Sci. 202 (2002) 47.
[24] M. Srivastava, A.K. Ojhaa, B.S. Chaubeya, A. Maternyb, J. Alloy. Compd. 481 (2009) 515.
[25] K.N. Harish, H.S. Bhojya Naik, P.N. Prashanth Kumar, R. Vishwanath, G. S. Yashvanth Kumar, Arch. of Appl. Sci. Res. 5 (2) (2013) 42.
[26] J. Tauc, *Plenum, New York*, **1974.** 159.
[27] S.V. Bangale, D.R. Patil, S.R. Bamane, Arch. of App. Sci. Res. 3 (5) (2011) 506.
[28] X. Wu, B. Zou, J. Xu, B. Yu, G. Tang, G. Zhang, W. Chen, Nanostruct. Mater. 8 (1997) 179.
[29] N. Kislov, S. S. Srinivasan, Yu. Emirov, E. K. Stefanakos, *Mater. Sci. Eng.*, B, 153, **2008,** 70.
[30] Y. Wu, S. Liu, Y. Zuo, J. Li, J. Wang, Catal. Lett. 119 (2007) 245.
[31] S. Horikoshi, A. Saitou, H. Hidaka, N. Serpone, Environ. Sci. Tech. 37 (2003) 5813.
[32] Z.X. Chen, D.Z. Li, W.J. Zhang, Y. Shao, T.W. Chen, M. Sun, X.Z. Fu, J. Phys. Chem. C 113 (2009) 4433.
[33] X. Li, Y. Hou, Q. Zhao, L. Wang, J. Colloid Interface Sci. 358 (2011) 102–108.
[34] K. N. Harish, H. S. Bhojya Naik, P. N. Prashanth kumar, and R. Viswanath, *ACS Sustainable Chem. Eng.* 1, 9, **2013**, 1143–1153.
[35] K. Karthik, D. Radhika, K.R. Reddy, A.V. Raghu, K.K. Sadasivuni, G. Palani, K. Gurushankar, Nano Ex. 1 (2) (2021), 010014.
[36] K.V. Karthik, C.V. Reddy, K.R. Reddy, R. Ravishankr, G. Sanjeev, R.V. Kulkarni, A. V. Raghu, J. Mater. Sci. Mater. Electron. 30 (2019) 20646–20653.
[37] Z. Khan, F. Ali, A. Said, U. Arif, K. Khan, N. Ali, G. Shabir, H.M.N. Iqbal, M. Bilal, Envir. Res. 215, Part 2 (2022), 114148.
[38] B. Mondal, M. Kundu, Siba Prasad Mandal, Rajat Saha, Ujjal Kanti Roy, Anirban Roychowdhury, and Dipankar Das, ACS Omega 4 (9) (2019) 13845–13852.
[39] Mousumi Kundu, Bibhas Mondal, Debjit Das, Ujjal Kanti Roy, Chemistry Select, 7, **2022**, e202104543.
[40] Bhaskar Jyoti Sarkar, Mousumi Kundu, Bibhas Mondal, Sunil Mukherjee, Atul Bandyopadhyay, Ujjal Kanti Roy, J. Mole. Stru. , 1274, Part 2, **2023**, 134493.